Assessment of Soil Moisture SMAP Retrievals and ELBARA-III Measurements in a Tibetan Meadow Ecosystem

Donghai Zheng, Xin Wang, Rogier van der Velde, Mike Schwank, Paolo Ferrazzoli, *Senior Member, IEEE*, Jun Wen, Zuoliang Wang, Andreas Colliander, *Senior Member, IEEE*, Rajat Bindlish, and Zhongbo Su

***Abstract*— This letter presents the results evaluating retrievals of liquid water content (θ_{liq}) performed with a zero-order radiative transfer (τ–ω) model under frozen and thawed soil conditions from Soil Moisture Active Passive (SMAP) and ELBARA-III brightness temperature (T_B^p) measurements collected over a Tibetan meadow ecosystem. A good agreement is found between time series of the SMAP and ELBARA-III measured T_B^p resulting in a Pearson product-moment coefficient (R) larger than 0.87. Differences noted between the two data sets can be associated with discrepancies in θ_{liq} measured in the specific footprints, whereby the SMAP measurements are best explained by the *in situ* θ_{liq}. Furthermore, the *in situ* θ_{liq} has a better agreement with the horizontally polarized SMAP and ELBARA-III measurements (T_B^H) in the cold season, whereas the vertically polarized measurements (T_B^V) are better correlated with θ_{liq} in the warm season. With the implementation of new vegetation and surface roughness parameterizations for the τ–ω model, the dynamics of *in situ* θ_{liq} is better reproduced by corresponding retrievals for both frozen and thawed soil conditions, leading to the reduction in the unbiased root-mean-square error (ubRMSE) by more than 31% in comparison with these retrievals using SMAP default parameterizations. Notably, the single-channel algorithm configured with the new parameterizations using SMAP T_B^V measured during the ascending overpass provides the best θ_{liq} retrievals with a ubRMSE of 0.035 $m^3 \cdot m^{-3}$ that is well within the SMAP mission requirements.**

***Index Terms*— Frozen and thawed soil, grassland, L-band microwave radiometry, liquid water content, Soil Moisture Active Passive (SMAP), Tibetan Plateau.**

Manuscript received September 11, 2018; revised January 12, 2019; accepted January 31, 2019. Date of publication March 5, 2019; date of current version August 27, 2019. This work was supported in part by the National Natural Science Foundation of China under Grant 41871273, Grant 41630856, and Grant 41530529, and in part by the Netherlands Organization for Scientific Research under Project ALW-GO/14-29. The work of D. Zheng was supported by the Chinese Academy of Sciences through Hundred Talent Program. *(Corresponding author: Donghai Zheng.)*

D. Zheng is with the Institute of Tibetan Plateau Research, Chinese Academy of Sciences, Beijing 100101, China (e-mail: zhengd@itpcas.ac.cn).

X. Wang and Z. Wang are with the Key Laboratory of Land Surface Process and Climate Change in Cold and Arid Regions, Northwest Institute of Eco-Environment and Resources, Chinese Academy of Sciences, Lanzhou 730000, China (e-mail: xinwang@lzb.ac.cn; zuoliangwang@lzb.ac.cn).

R. van der Velde and Z. Su are with the Faculty of Geo-Information Science and Earth Observation, University of Twente, 7500 AE Enschede, The Netherlands (e-mail: r.vandervelde@utwente.nl; z.su@utwente.nl).

M. Schwank is with the Swiss Federal Research Institute WSL, 8903 Birmensdorf, Switzerland (e-mail: mike.schwank@wsl.ch).

P. Ferrazzoli is with the Dipartimento di Ingegneria Civile e Ingegneria Informatica, Via del Politecnico, University of Rome Tor Vergata, 00133 Rome, Italy (e-mail: paolo.ferrazzoli@uniroma2.it).

J. Wen is with the College of Atmospheric Sciences, Plateau Atmosphere and Environment Key Laboratory of Sichuan Province, Chengdu University of Information Technology, Chengdu 610225, China (e-mail: jwen@lzb.ac.cn).

A. Colliander is with the Jet Propulsion Laboratory, California Institute of Technology, Pasadena CA 91109 USA (e-mail: andreas.colliander@jpl.nasa.gov).

R. Bindlish is with the Hydrological Sciences Laboratory, Goddard Space Flight Center, NASA, Greenbelt, MD 20771 USA (e-mail: rajat.bindlish@nasa.gov).

Color versions of one or more of the figures in this letter are available online at http://ieeexplore.ieee.org.

Digital Object Identifier 10.1109/LGRS.2019.2897786

I. Introduction

FOR the assessment of the brightness temperature (T_B^p) measurements collected by the Soil Moisture and Ocean Salinity (SMOS) and Soil Moisture Active Passive (SMAP) missions, numerous validation campaigns with ground- or aircraft-mounted L-band radiometers have been carried out over various land covers and climate zones. Examples of such field campaigns are: 1) MELBEX III vine vegetation site in Valencia, Spain [1]; 2) boreal and subarctic environmental site in Sodankylä, Finland [2]; 3) SMOS validation campaign in the Rur and Erft catchment, Germany [3]; and 4) SMAPEx [4], SMAPVEX12 [5], and SMAPVEX15 [6] field campaigns conducted in Australia, Canada, and USA, respectively. These experiments have been used specifically to evaluate and improve the soil moisture processors developed as part of the SMOS and SMAP missions [7], [8]. Furthermore, the SMAP mission has also utilized a set of core validation sites across diverse vegetation types and climatic regions to evaluate the mission's performance [9].

The research presented in this letter is conducted under the same validation framework in one of the validation sites on the high Tibetan Plateau selected by the SMAP scientific team [9], namely, the Maqu *in situ* soil moisture and soil temperature (SMST) network that is representative of a typical Tibetan meadow ecosystem [10]. As part of the SMAP and SMOS calibration/validation activities, one of the European Space Agency-funded ELBARA-III radiometers [11] has been deployed within the SMST network to measure

the T_B^p variations every 30 min [12]. Although the spatial footprints of spaceborne and ground-based radiometers are very different, e.g., several square meters versus thousands of square kilometers, Wigneron *et al.* [7] showed that the ground-based T_B^p measurements are still useful for the analysis of spaceborne radiometer signatures measured over similar land covers. For this letter, the footprints of both SMAP and ELBARA-III are homogeneous and mainly covered by alpine meadows.

In a recent analysis of both SMAP T_B^p and *in situ* SMST data measured at the Maqu site, Zheng *et al.* [13] showed that the soil moisture retrieval algorithm implemented by the SMAP mission overestimates the vegetation effect and underestimates the surface roughness effect over the Tibetan Plateau. As a result, new parameterizations have been proposed to mitigate these deficiencies. In addition, Zheng *et al.* [13] showed that the updated SMAP algorithm configured with the four-phase refractive dielectric model [14] expressing the soil permittivity (ε_s) as a function of soil liquid water content (θ_{liq}) can be used to retrieve θ_{liq} for both frozen and thawed soil conditions, whereas current SMAP and SMOS soil moisture products are only available for thawed soils. However, the analysis of SMAP T_B^p measurements reported by Zheng *et al.* [13] is limited to data obtained from the descending overpass.

In this letter, we expand the retrieval algorithm introduced by Zheng *et al.* [13] to both descending (morning) and ascending (afternoon) overpasses. Tests of the algorithm are also extended in time and spatial resolution, as a new interval (2016–2017) and ELBARA-III measurements have been included. Furthermore, θ_{liq} retrievals are derived from SMAP and ELBARA-III T_B^p measurements in order to identify the optimum retrieval combinations yielding reliable θ_{liq} estimates for both frozen and thawed soil conditions over the Plateau.

II. Field Site and Measurements

The Maqu *in situ* SMST network is located in the source area of Yellow River on the northeast Tibetan Plateau (Fig. 1) that contributes to more than 35% of the total streamflow of Yellow River. The network holds 30 SMST profile measurement stations, and each station records every 15-min readings of 5TM ECH_2O probes installed at soil depths of 5, 10, 20, 40, and 80 cm. The ELBARA-III radiometer has been deployed in the center of the SMST network (Fig. 1) at the beginning of 2016. The L-band radiometer is installed on a 4.8-m tower with an antenna beam waist about 6.5 m above the ground. The T_B^p measurements of the ground at horizontal (T_B^H) and vertical polarizations (T_B^V) are performed every 30 min for observation angles of 40°–70° in steps of 5°. The horizontal distances measured from the radiometer tower to the closest (d_{min}) and farthest (d_{max}) borders of the antenna footprint are 4.38 and 26.07 m, respectively. Concurrent to the ELBARA-III T_B^p measurements, SMST profiles are measured next to the radiometer tower. Detailed descriptions of the SMST network and ELBARA-III field site are outlined in [12] and [13].

Version 3 of the Level 1C SMAP radiometer product has been used for the presented research, and the SMAP pixel has been centered on the Maqu network as has been done for all the core validation sites [9] to reduce the uncertainties associated with spatial misalignment of the *in situ* references and the retrievals. Fig. 1 shows that the ELBARA-III field site is located at the top right corner of the SMAP pixel.

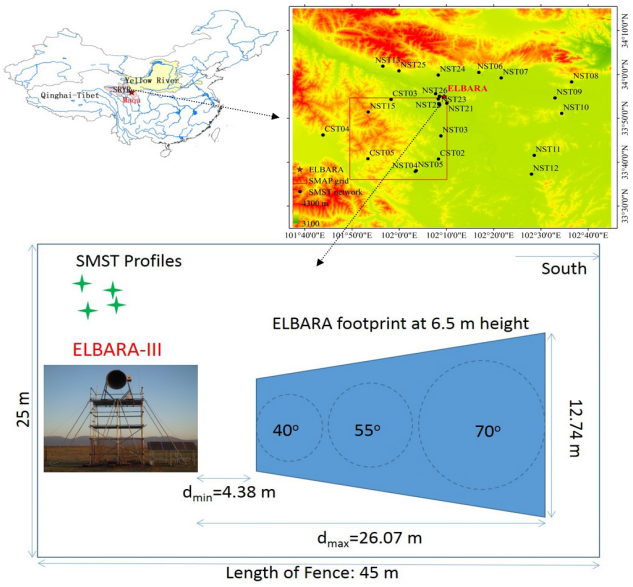

Fig. 1. Location of the ELBARA-III field site and the Maqu SMST monitoring network in the source region of Yellow River. The red box in the top right map indicates the boundary of selected SMAP pixel.

The SMAP T_B^p measurements during both descending (6 A.M.) and ascending (6 P.M.) overpasses are used, and the data collected from August 2016 to July 2017 are extracted for the SMAP pixel, which sums up to 360 SMAP measurements available for analysis.

III. Model and Algorithms

The single-channel algorithm (SCA) using T_B^V measurements (SCA-V) is the baseline soil moisture retrieval algorithm implemented by the SMAP mission, whereby the τ–ω model based on the zero-order radiative transfer approach is adopted to simulate the microwave emission from land [15]. Recently, Zheng *et al.* [13] implemented the four-phase dielectric mixing model [14] enabling the retrieval of θ_{liq} under both frozen and thawed soil conditions. In addition, new vegetation and surface roughness parameterizations have been proposed to mitigate the overestimation of vegetation effect and underestimation of surface roughness effect found when using the default SMAP parameterizations for the Tibetan environment. Table I lists the SMAP default and the new vegetation and surface roughness parameterizations for the Tibetan grassland, whereby the leaf area index (LAI) and normalized difference vegetation index (NDVI) are obtained from the MODIS MOD15A2 [16] and MOD13A2 [17] products, respectively. In this letter, the SCA-V algorithm in combination with the four-phase dielectric mixing model is configured with either the SMAP default or the new parameterizations of vegetation and surface roughness to retrieve θ_{liq} as in [13].

IV. Results

A. Comparisons of SMAP and ELBERA-III Measurements

Fig. 2(a) shows the SMAP and ELBARA-III measured T_B^p during the SMAP descending overpass from August 2016 to July 2017. The shown ELBARA-III T_B^p measurements have been collected at an incidence angle of 40° and at the time closest to the SMAP overpasses, and the data gap is caused by a power supply failure. Table II lists the statistical errors calculated between the SMAP and ELBARA-III

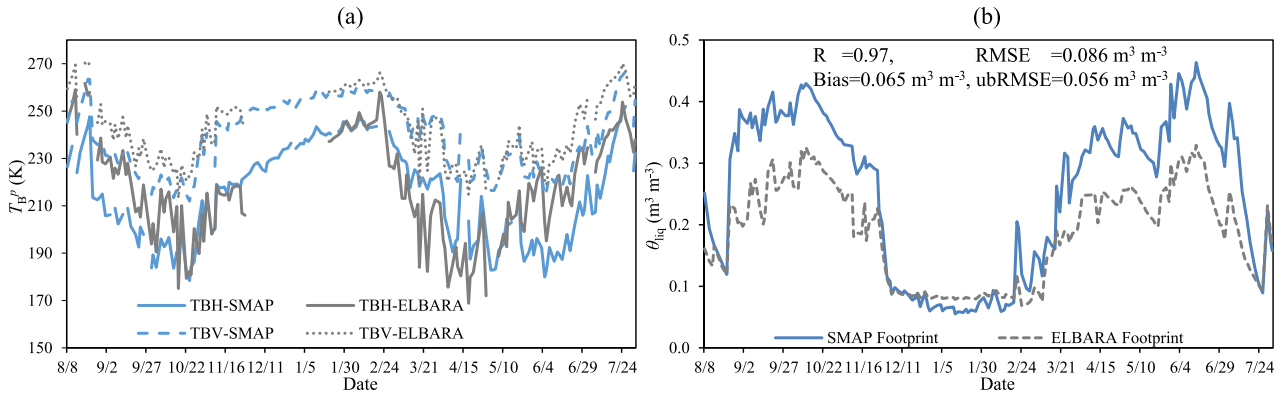

Fig. 2. Time series of (a) ELBARA-III- and SMAP measured T_B^p and (b) the average θ_{liq} measured at a depth of 5 cm within the ELBRA-III and SMAP footprints during the SMAP descending overpass from August 2016 to July 2017.

TABLE I

SUMMARY OF SMAP DEFAULT AND THE NEW VEGETATION AND SURFACE ROUGHNESS PARAMETERIZATIONS ADOPTED IN THIS LETTER FOR THE TIBETAN GRASSLAND

τ-ω model component*	SMAP parameterization[15]	New parameterization[13]
τ	$\tau = b \cdot VWC$, $b = 0.13$ $VWC = 1.9134 \cdot NDVI^2 - 0.3215 \cdot NDVI + 1.5 \cdot (NDVI - 0.1)/(1 - 0.1)$	$\tau = 0.025 \cdot LAI$
ω	$\omega = 0.05$	
h	$h = 0.01 \cdot s = 0.156$	$h = \left(\frac{0.9437 \cdot s}{0.8865 \cdot s + 2.2913}\right)^6 = 0.58$
Q	$Q = 0$	$Q = 0.1771 \cdot h = 0.1$
N	$N = 2$	

*τ is the vegetation optical depth, ω is the effective scattering albedo, VWC is the vegetation water content, h represents the intensity effect of surface roughness, Q represents the polarization mixing effect, N represents the angular effect, and s is the surface height standard deviation specified as 15.6 mm for the grassland.

TABLE II

STATISTICAL ERRORS CALCULATED BETWEEN SMAP AND ELBARA-III T_B^p MEASUREMENTS BETWEEN AUGUST 2016 AND JULY 2017

T_B^p	ubRMSE (K)	Bias (K)	RMSE (K)	R
		Descending		
T_B^H	15.00	-4.09	15.55	0.73
T_B^V	7.19	-4.97	8.74	0.88
		Ascending		
T_B^H	13.99	-4.09	14.58	0.87
T_B^V	7.10	-6.53	9.65	0.92

measurements, i.e., Pearson product-moment correlation coefficient (R), bias, root-mean-square error (RMSE), and unbiased RMSE (ubRMSE). Furthermore, Fig. 2(b) shows the time series of spatial mean of *in situ* measured θ_{liq} taken at a 5-cm soil depth within the SMAP (Fig. 1, 12 SMST sites) and the ELBARA-III (4 SMST sites) footprints. The statistical errors computed between the *in situ* θ_{liq} representative of the SMAP and ELBARA-III footprints are also given in Fig. 2(b).

The dynamics of the average θ_{liq} measured within the SMAP footprint are comparable with those of ELBARA-III footprint with a high R value ($R = 0.97$). The soil is generally wet and unfrozen during the warm season between May and October, whereas it appears as dry during the cold period between November and April with mostly frozen soil. It can be noted that the average θ_{liq} measured within the SMAP

TABLE III

PEARSON PRODUCT-MOMENT CORRELATION COEFFICIENTS (R) CALCULATED BETWEEN T_B^p, PR DERIVED FROM BOTH SMAP AND ELBRA-III MEASUREMENTS, AND THE AVERAGE θ_{liq} MEASURED AT A DEPTH OF 5 cm WITHIN THE SMAP AND ELBRA-III FOOTPRINTS DURING THE WARM (MAY–OCTOBER) AND COLD (NOVEMBER–APRIL) SEASONS

R^2	SMAP_ Warm	SMAP_ Cold	ELBARA_ Warm	ELBARA_ Cold
		Descending		
T_B^H	0.89	0.89	0.75	0.84
T_B^V	0.92	0.96	0.90	0.81
PR	0.77	0.83	0.27	0.81
		Ascending		
T_B^H	0.90	0.92	0.80	0.80
T_B^V	0.92	0.92	0.91	0.78
PR	0.78	0.90	0.40	0.79

footprint is larger than that of the ELBARA-III footprint during the warm season, due to the soil heterogeneity found across the SMAP footprint including organic soil with a high water holding capacity [18]. A comparison of Fig. 2(a) and (b) indicates that both SMAP and ELBARA-III measured T_B^H and T_B^V variations follow the dynamics of the *in situ* θ_{liq} during the warm season, with the T_B^H and T_B^V decreasing as the θ_{liq} increases (e.g., in September 2016) and vice versa (e.g., in July 2017). In addition, the freezing of the soil (lower θ_{liq}) leads to the increase in both T_B^H and T_B^V between November and February, and the thawing of soil ice results in the decrease in T_B^p between February and April. In general, high R values ($R \geq 0.87$) are found between the SMAP and ELBARA-III T_B^p measurements except for T_B^H obtained during the SMAP descending overpass. It can also be found that the SMAP T_B^p measurements are lower than those measured by the ELBARA-III during the warm season, which can be explained by the fact that the average θ_{liq} measured in the SMAP footprint is larger than that of the ELBARA-III footprint.

In support of further analysis, Table III shows the Pearson product-moment correlation coefficient estimated between T_B^H, T_B^V, and polarization ratio [PR $\equiv (T_B^V - T_B^H)/(T_B^V + T_B^H)$] derived from the SMAP and ELBARA-III measurements and the corresponding footprint θ_{liq} averages. The statistics is performed for the warm (May–October) and cold (November–April) seasons, separately. The SMAP measurements (i.e., T_B^H, T_B^V, and PR) generally show better agreements with the *in situ* θ_{liq} average with higher R values

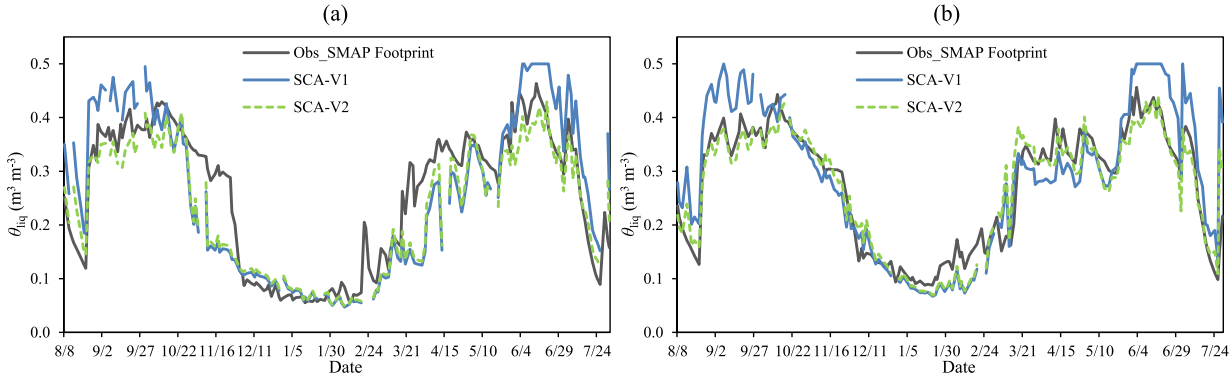

Fig. 3. Time series of the *in situ* θ_{liq} averages and retrievals produced with the SCA-V approach using SMAP measurements for the SMAP (a) Descending and (b) Ascending overpasses from August 2016 to July 2017. SCA-V1: SMAP default parameterization and SCA-V2: new parameterization proposed by Zheng *et al.* [13].

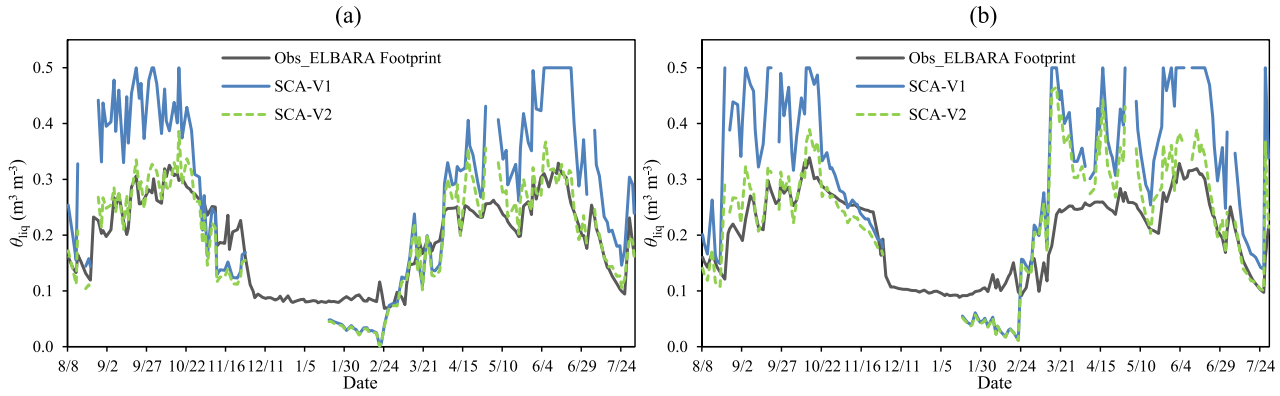

Fig. 4. Time series of the *in situ* θ_{liq} averages and retrievals produced with the SCA-V approach using ELBARA-III measurements for the SMAP (a) Descending and (b) Ascending overpasses. SCA-V1: SMAP default parameterization and SCA-V2: new parameterization proposed by Zheng *et al.* [13].

in comparison with the ELBARA-III measurements. For the warm season, both SMAP and ELBARA-III measured T_B^V are better correlated with the θ_{liq} measurements with R values larger than 0.90, whereas somewhat higher R values are found between the T_B^H measurements and the *in situ* θ_{liq} for the cold season.

B. Retrieval of Soil Liquid Water Content

The SCA-V approach in combination with the four-phase dielectric mixing model (Section III) is configured with either the SMAP default (hereafter "SCA-V1") or the new (SCA-V2) vegetation and surface roughness parameterizations (Table I) to assess their effects on retrieving θ_{liq}. Both SMAP and ELBARA-III T_B^V measurements collected during the SMAP descending and ascending overpasses are used for identifying the optimum retrieval combinations for both cold and warm seasons.

Fig. 3 shows the time series of averaged θ_{liq} derived from measurements taken at a 5-cm soil depth within the SMAP footprint (black line) for the period between August 2016 and July 2017. Time series of θ_{liq} retrieved with the SCA-V1 and SCA-V2 approaches are shown as colored lines. Corresponding statistical errors computed using the measured and retrieved θ_{liq} are given in Table IV. The SCA-V1 overestimates θ_{liq} in the warm season due to the T_B^p overestimations as was previously documented in [13]. After implementing the new vegetation and surface roughness parameterizations, this discrepancy is largely reduced, and the measured θ_{liq} dynamics are better captured as indicated by the SCA-V2 estimates. A comparison of the error statistics achieved with SCA-V1 and SCA-V2 indicates that the new vegetation and surface roughness parameterizations reduce the ubRMSE computed between the *in situ* and retrieved θ_{liq} by about 36% on average. Notably, the SCA-V2 using the SMAP T_B^V measured during the ascending overpass provides the retrievals that best match the average θ_{liq} measured within the SMAP footprint. For this case (SMAP T_B^V and ascending overpass), an ubRMSE value of 0.035 $m^3 \cdot m^{-3}$ is obtained, which is well within the SMAP mission goal of an ubRMSE = 0.04 $m^3 \cdot m^{-3}$[15].

Fig. 4 shows the time series of the average θ_{liq} measured at a 5-cm soil depth within the ELBARA-III footprint (black line), and θ_{liq} retrieved with the SCA-V approach using the ELBARA-III measurements at the off-nadir angle of 40° is shown with the colored lines. Statistical errors calculated between the *in situ* and retrieved θ_{liq} are given in Table IV as well. As is the case for the SMAP-based retrievals, the SCA-V2 improves the θ_{liq} overestimation in the warm season noted for the SCA-V1 using the ELBARA-III measurements, which is reflected in the superior error statistics presented in Table IV. It can also be noted that the θ_{liq} retrievals produced using the SMAP measurements capture better the measured θ_{liq} dynamics in comparison with the performance of these retrievals produced based on the ELBARA-III measurements (Table IV).

TABLE IV

STATISTICAL ERRORS CALCULATED BETWEEN THE *In Situ* θ_{liq} AVERAGES AND RETRIEVALS PRODUCED WITH THE SCA-V APPROACH BASED ON EITHER SMAP OR ELBARA-III MEASUREMENTS. SCA-V1: SMAP DEFAULT PARAMETERIZATION AND SCA-V2: NEW PARAMETERIZATION PROPOSED BY ZHENG *et al.* [13]

Retrievals	SMAP Footprint				ELBARA Footprint			
	ubRMSE (m^3 m^{-3})	Bias (m^3 m^{-3})	RMSE (m^3 m^{-3})	R	ubRMSE (m^3 m^{-3})	Bias (m^3 m^{-3})	RMSE (m^3 m^{-3})	R
Descending								
SCA-V1	0.076	-0.001	0.076	0.86	0.093	0.069	0.116	0.88
SCA-V2	0.052	-0.027	0.059	0.92	0.043	-0.002	0.044	0.91
Ascending								
SCA-V1	0.058	0.017	0.061	0.90	0.098	0.092	0.134	0.83
SCA-V2	0.035	-0.005	0.035	0.95	0.065	0.021	0.068	0.83

V. CONCLUSION

This letter presents an assessment of θ_{liq} retrievals for both frozen and thawed soils from spaceborne and ground-based L-band microwave radiometer measurements (i.e., SMAP and ELBARA-III) for a Tibetan meadow ecosystem. In the first step, we compare the SMAP and ELBARA-III T_B^p measurements at the off-nadir observation angle of 40° for a full annual cycle between August 2016 and July 2017. In spite of significantly different footprints, a good agreement ($R \geq 0.87$) is found between the two data sets except for the T_B^H measurement obtained during the SMAP descending overpass, for which R equals 0.73. Discrepancies noted between the SMAP and ELBARA-III measurements can be related to the systematic differences between *in situ* θ_{liq} measured within the SMAP and ELBARA-III footprints.

In the second step, we evaluate the performance of the SCA-V approach in retrieving θ_{liq} using the default SMAP surface roughness and vegetation parameterizations, and a parameterization recently found to be better suited for the Tibetan alpine meadows. Adopting this new surface roughness and vegetation parameterization leads to better θ_{liq} retrievals for both cold and warm seasons in comparison with *in situ* θ_{liq} measured within the SMAP and ELBARA-III footprints. It can also be noted that the SMAP-based θ_{liq} retrievals capture better *in situ* measurements in comparison with the ELBARA-III estimates. Notably, the SCA approach configured with the new parameterization using the SMAP T_B^V measurement obtained during the ascending overpass provides the best θ_{liq} retrievals with an ubRMSE of 0.035 $m^3 \cdot m^{-3}$ that is well within the SMAP mission requirements of an ubRMSE of 0.04 $m^3 \cdot m^{-3}$.

This letter demonstrates the potential of the SCA-V applied to satellite-based L-band microwave radiometer measurements for producing reliable θ_{liq} estimates for both frozen and thawed soil conditions in a Tibetan meadow ecosystem. Additional effort would, however, be needed to extend and confirm above findings for large spatial domains and other land covers, such as the entire Tibetan Plateau. Improved θ_{liq} retrievals under both frozen and thawed soil conditions across the Tibetan Plateau would greatly assist in quantifying water and heat exchanges in this region and their impact on regulating the regional climate and water cycle of East and Southeast Asia [19].

ACKNOWLEDGMENT

The authors would like to thank the European Space Agency for providing ELBARA-III instrument.

REFERENCES

[1] M. Schwank, J.-P. Wigneron, E. López-Baeza, I. Völksch, C. Mätzler, and Y. H. Kerr, "L-band radiative properties of vine vegetation at the MELBEX III SMOS cal/val site," *IEEE Trans. Geosci. Remote Sens.*, vol. 50, no. 5, pp. 1587–1601, May 2012.

[2] K. Rautiainen *et al.*, "L-band radiometer observations of soil processes in boreal and subarctic environments," *IEEE Trans. Geosci. Remote Sens.*, vol. 50, no. 5, pp. 1483–1497, May 2012.

[3] C. Montzka *et al.*, "Brightness temperature and soil moisture validation at different scales during the SMOS validation campaign in the Rur and Erft catchments, Germany," *IEEE Trans. Geosci. Remote Sens.*, vol. 51, no. 3, pp. 1728–1743, Mar. 2013.

[4] R. Panciera *et al.*, "The soil moisture active passive experiments (SMAPEx): Toward soil moisture retrieval from the SMAP mission," *IEEE Trans. Geosci. Remote Sens.*, vol. 52, no. 1, pp. 490–507, Jan. 2014.

[5] H. McNairn *et al.*, "The soil moisture active passive validation experiment 2012 (SMAPVEX12): Prelaunch calibration and validation of the SMAP soil moisture algorithms," *IEEE Trans. Geosci. Remote Sens.*, vol. 53, no. 5, pp. 2784–2801, May 2015.

[6] A. Colliander *et al.*, "Validation and scaling of soil moisture in a semi-arid environment: SMAP validation experiment 2015 (SMAPVEX15)," *Remote Sens. Environ.*, vol. 196, pp. 101–112, Jul. 2017.

[7] J.-P. Wigneron *et al.*, "First evaluation of the simultaneous SMOS and ELBARA-II observations in the Mediterranean region," *Remote Sens. Environment*, vol. 124, pp. 26–37, Sep. 2012.

[8] J. P. Wigneron *et al.*, "Modelling the passive microwave signature from land surfaces: A review of recent results and application to the L-band SMOS & SMAP soil moisture retrieval algorithms," *Remote Sens. Environ.*, vol. 192, pp. 238–262, Apr. 2017.

[9] A. Colliander *et al.*, "Validation of SMAP surface soil moisture products with core validation sites," *Remote Sens. Environ.*, vol. 191, pp. 215–231, Mar. 2017.

[10] Z. Su *et al.*, "The tibetan plateau observatory of plateau scale soil moisture and soil temperature (Tibet-Obs) for quantifying uncertainties in coarse resolution satellite and model products," *Hydrol. Earth Syst. Sci.*, vol. 15, no. 7, pp. 2303–2316, 2011.

[11] M. Schwank *et al.*, "ELBARA II, an L-band radiometer system for soil moisture research," *Sensors*, vol. 10, no. 1, pp. 584–612, 2010.

[12] D. Zheng *et al.*, "L-band microwave emission of soil freeze–thaw process in the third pole environment," *IEEE Trans. Geosci. Remote Sens.*, vol. 55, no. 9, pp. 5324–5338, Sep. 2017.

[13] D. Zheng *et al.*, "Impact of surface roughness, vegetation opacity and soil permittivity on L-band microwave emission and soil moisture retrieval in the third pole environment," *Remote Sens. Environ.*, vol. 209, pp. 633–647, May 2018.

[14] M. Schwank, M. Stahli, H. Wydler, J. Leuenberger, C. Matzler, and H. Fluhler, "Microwave L-band emission of freezing soil," *IEEE Trans. Geosci. Remote Sens.*, vol. 42, no. 6, pp. 1252–1261, Jun. 2004.

[15] P. O'Neill, E. Njoku, T. Jackson, S. Chan, and R. Bindlish, "SMAP algorithm theoretical basis document: Level 2 & 3 soil moisture (passive) data products," Jet Propulsion Lab., California Inst. Technol., Pasadena, CA, USA, Tech. Rep. JPL D-66480, 2015.

[16] R. Myneni, Y. Knyazikhin, and T. Park, "MCD15A3H MODIS/Terra+Aqua leaf area index/FPAR 4-day L4 global 500 m SIN Grid V006," NASA EOSDIS land processes DAAC, College Park, MD, USA, Tech. Rep., 2015.

[17] A. R. Huete, K. Didan, T. Miura, E. P. Rodriguez, X. Gao, and L. G. Ferreira, "Overview of the radiometric and biophysical performance of the MODIS vegetation indices," *Remote Sens. Environ.*, vol. 83, nos. 1–2, pp. 195–213, 2002.

[18] D. Zheng *et al.*, "Augmentations to the Noah model physics for application to the yellow river source area. Part I: Soil water flow," *J. Hydrometeorol.*, vol. 16, pp. 2659–2676, Dec. 2015.

[19] D. Zheng *et al.*, "Impacts of Noah model physics on catchment-scale runoff simulations," *J. Geophys. Res., Atmos.*, vol. 121, pp. 807–832, Jan. 2016.